NUMERICAL PREDICTIONS AND EXPERIMENTS ON SUPERSONIC JET MIXING FROM CASTELLATED NOZZLES

A. J. Saddington, N. J. Lawson, K. Knowles
Aeromechanical Systems Group
Department of Aerospace, Power and Sensors
Cranfield University, RMCS Shrivenham
Swindon, Wiltshire, SN6 8LA, UK.

Keywords: *Jet, mixing, underexpanded, supersonic, turbulent, CFD, LDV.*

Abstract

This work presents a numerical and experimental study of mixing in underexpanded, supersonic turbulent jets issuing from axisymmetric and castellated nozzles into quiescent conditions. Experimental studies used laser doppler velocimetry (LDV) and pitot probe measurements along the jet centreline at a nozzle pressure ratio (NPR) of 4. A computational fluid dynamics (CFD) model using the Fluent commercial code (v5.5) and the RNG k-ε two-equation turbulence model was developed. Comparison of the jet centreline LDV and pitot probe data showed good agreement with the CFD model. In agreement with the experimental data, the CFD predicted a shortening of the shock cells in the jets emanating from the castellated nozzles. The degree to which the shock cells were shortened by the castellated nozzles was also in agreement with the experiments. When compared with a plain axisymmetric jet, an increase of up to 13% in mixing, based on mass flow rate, was predicted for jets emanating from the castellated nozzles. The increased mixing rate of these jets appears to be due to differential expansion of the jet fluid in the gap and tooth regions as it leaves the nozzle exit. This mixing enhancement was, however, confined to the nearfield flow $(x/D < 10)$. At greater streamwise distances viscous dissipation appeared to cause the entrainment mechanism to decay resulting in mixing rates similar to an axisymmetric jet.

Nomenclature

CFD	computational fluid dynamics
D	nozzle exit diameter (0.0294 m)
ℓ	mixing length
LDV	laser doppler velocimetry
$\dot{m}$	mass flow rate
M	Mach number
NPR	nozzle pressure ratio $\left\{ \frac{p_{0c}}{p_a} \right\}$
p	static pressure
p_a	atmospheric static pressure
p_0	total pressure
p_{0c}	settling chamber total pressure
p_{0p}	pitot probe pressure
r	radial distance from nozzle centreline
T	static temperature
T_a	atmospheric static temperature
T_i	turbulence intensity $\left\{ \frac{\sqrt{\frac{1}{3}\left(u'^2+v'^2+w'^2\right)}}{V_{ref}} \right\}$
u	axial velocity
u_θ	tangential velocity
v	vertical velocity (see Fig. 3)
V_{ref}	reference velocity (speed of sound)
w	horizontal velocity (see Fig. 3)
x	axial distance from nozzle exit
$()'$	e.g. u', fluctuating velocity component
$()_{rms}$	e.g. u_{rms}, rms velocity component

1 Introduction

The rate at which a supersonic jet mixes with the surrounding ambient fluid is important for many aerospace applications, notably in jet aircraft and rocket propulsion. For these applications enhanced mixing is often highly desirable, for example to reduce jet noise, improve thrust augmentation or to improve combustion chamber design in scramjets.

For aircraft propulsion applications, passive control has the advantage of robustness and minimal power requirement. For supersonic jets the generation of streamwise vortices appears to be beneficial [7] and schemes have been investigated using vortex generators, tabs [8] and other intrusive devices. Nozzle lip or trailing edge modifications have been shown in previous studies to have a dramatic effect on jet development. For example, triangular notches in the nozzle lip generate strong streamwise vortices and distort the jet cross-section [4].

This paper reports on experimental and computational fluid dynamics (CFD) investigations into three castellated nozzle designs, where the nozzle lip is non-planar but there are no intrusions into the jet stream. Such nozzles appear to generate streamwise vortices at underexpanded conditions by differential expansion between castellation and gap [3]. As such, they work well in underexpanded conditions but their performance deteriorates as the nozzle is operated closer to correctly expanded. The mixing performance of the castellated nozzles was normalised to that of a plain axisymmetric nozzle.

2 Objectives

The objectives of this study were to take LDV velocity and turbulence measurements of the flow issuing from two different circular convergent under-expanded castellated nozzles and, together with pitot probe data for a third castellated nozzle, compare the data with a CFD model of the experiments. Mixing enhancement would be determined by comparison with data for a plain axisymmetric nozzle [6]. The aim was to ascertain the ability of the CFD model to adequately predict the shock cell structure, the length of the shock core and the previously reported mixing enhancement seen with such nozzle designs [2].

3 Methodology

3.1 Nozzle Design

Three castellated nozzles with convergent profiles were investigated (Fig. 1). Each nozzle had four regularly spaced castellations. The difference between the three nozzles was confined to the geometry of the gap between each castellation.

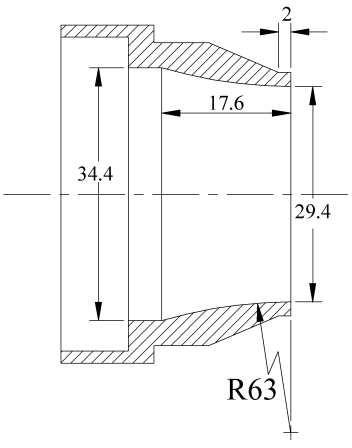

Fig. 1 Nozzle geometry showing the internal profile.

The first nozzle (regular) had castellations cut by a radial line from the centre of the nozzle, as shown by the inner region of Fig. 2. The ‘outer region’ of Fig. 2 indicates alternative tooth designs (for all four teeth); radial position is as the ‘inner region’. The second nozzle (divergent chamfered) had castellations cut such that the gap between each nozzle was divergent in profile, as indicated by the ‘*’ on the outer region of Fig. 2. The third nozzle (convergent chamfered) had castellations cut such that the gap between each profile was convergent in profile, as indicated by the ‘**’ on the outer region of Fig. 2. The plain axisymmetric nozzle was of the same overall geometry as the castellated ones but with the gaps between the teeth ‘filled in’ [6].

The mixing enhancement obtained from these three nozzle geometries was to be compared with an axisymmetric convergent nozzle [6].

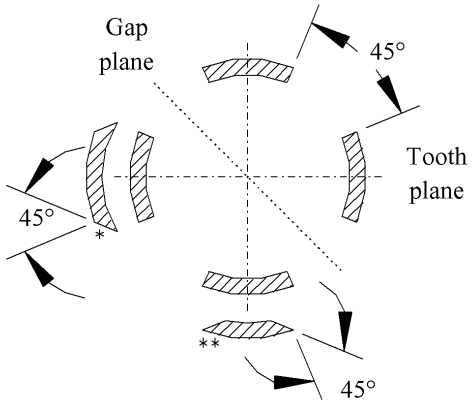

Fig. 2 Nozzle castellation configurations. Hatched boxes indicate locations of teeth in nozzle lip: (*) alternative profile for divergent chamfered castellations; (**) alternative profile for convergent chamfered castellations.

3.2 Experiments

Experiments were conducted in a nozzle test cell at Shrivenham (Fig. 3). Two Howden rotary screw compressors running in series supplied compressed dried air at a pressure of 6.9 bar (gauge) and a flow rate of 1.02 kgs^{-1} to a small plenum chamber in this cell, which is just visible in the bottom right hand corner of Fig. 3. For the jet experiments reported here, the compressors were run continuously and discharged to atmosphere, with the required jet air supply being bled off to a 34.4 mm internal diameter, 152 mm long jet pipe to which each test nozzle was attached (Fig. 3).

Jet total pressure, p_{0c} was measured using a pitot tube (within the jet supply pipe) and adjusted with a gate valve, which controlled the proportion of the compressed air supply that was discharged to atmosphere. Using this method, the NPR could be set to an accuracy of ± 0.1. Flow temperature was measured with a thermometer

Fig. 3 LDV measurements in the nozzle test cell.

mounted indirectly in the jet rig supply pipe. The jet air was exhausted from the test cell through a 0.3 m diameter hole via a 45° capture cone, which was 0.42 m downstream of the nozzle exit (Fig. 3). Data were collected for NPR = 4.

Three-dimensional LDV measurements were taken of the flow from the regular and divergent chamfered castellated nozzles using a Dantec system based on FibreFlow optics, two 300 mm focal length probes, three BSA enhanced signal processors and Dantec Burstware software. The probes were set-up with beam separations of 20 mm giving probe volumes of 150 μm $\times$ 150 μm $\times$ 2.8 mm. The processors were set to non-coincidence mode to ensure acceptable data rates in u, v and w. Seeding of the jet was by direct injection from a TSI six-jet seeder into the plenum chamber using JEM Hydrosonic seeding fluid.

Measurement traverses were made along the nozzle centreline, across the nozzle exit plane and across the jet at one, two, five and 10 diameters downstream of the exit. Each measurement point was sampled for 5 seconds and contained between 1000 and 3000 samples to yield u, v, and w mean velocities and u_{rms}, v_{rms} and w_{rms} turbulence data. Probe access limited data collection to within $10D$ of the nozzle exit plane. The LDV measurements were estimated to be accurate to $\pm 1\%$ of velocity based on the sample time and frequency.

Additional comparative data were taken from centreline LDV measurements of the plain ax-

isymmetric nozzle [6] and pitot probe measurements of the convergent chamfered castellated nozzle [2, 9] made previously under the same test conditions. The pitot probe was mounted on a 2D travelling microscope carriage modified to accommodate a stepper motor on each axis. The carriage was driven with a traverse range of 120 mm. Physical carriage location could be verified using vernier scales mounted on each axis. The traverse plane was parallel to the jet axis, enabling centre-line pitot pressure profiles to be obtained. The limited travel of the carriage required the rig to be repositioned downstream to give coverage of the whole jet. Thus, centreline pressure profiles consist of two plots taken at different times. Data points were recorded at 2 mm intervals along the jet centreline. Probe access limited the extent of measurements to just under $8D$.

3.3 Numerical Model

The CFD model was developed using the Fluent commercial code (Version 5.5). The computational domain consisted of a three dimensional hexahedral mesh with approximately 250,000 to 450,000 cells depending on the test conditions. Only one quarter of the geometry was modelled since each nozzle has two axes of symmetry. The inlet plane was approximately $1D$ upstream of the nozzle exit, the outlet plane was at about $50D$ downstream and the radial boundary diverged from $2D$ at the upstream end to more than $10D$ downstream.

The boundary condition for the nozzle inlet was set as a pressure inlet with a prescribed total pressure, static pressure, total temperature and turbulence intensity. The turbulence intensity, T_i at nozzle inlet in the CFD model was adjusted to give the same nozzle exit turbulence intensity as the experiments (approximately 4%). The experimental T_i was derived from the rms velocity data measured by the LDV technique. The turbulence length scale was set as 7.5% of nozzle radius [5]. The farfield boundary was set as a pressure outlet with a prescribed static pressure and static temperature. The boundary conditions are summarised in Table 1.

Boundary condition	Variable	Magnitude
Nozzle inlet	p_0	NPR $\times$ p_a
	p	p_a
	T	T_a
	T_i	From LDV
	ℓ	$0.075\,(D/2)$
Farfield	p	p_a
	T	T_a

Table 1 Summary of the boundary conditions for the CFD model.

Turbulent calculations were performed using the RNG k-ε turbulence model [10], which has been shown to be suitable for modelling underexpanded jets [1].

Initial axisymmetric calculations were conducted on a mesh of 14700 cells. Three stages of mesh adaption, based on density gradients greater than 1×10^{-5} (to capture the shear layer) and Mach numbers greater than 1.0 (to capture the shock core), were then performed. This reduced the grid spacing in the shock cell regions from 2 mm to 0.25 mm. Three stages of mesh adaption were sufficient to ensure a grid-independent solution [6].

Calculations were performed using a multi-stage (Runge-Kutta) solver employing a full approximation storage multi-grid scheme with five levels to accelerate the multi-stage solver. CFD models were developed for the axisymmetric nozzle and all three castellated nozzle designs.

4 Results

The results from the CFD model were compared with the LDV and pitot probe measurements as discussed below.

4.1 Centreline Axial Velocity Measurements

Fig. 4 shows the variation in jet centreline axial velocity with x/D for the LDV data at a NPR of 4. Up to seven shock cells were captured by the

LDV. Shock cell length was defined as the distance between subsequent velocity peaks. There are clear differences between the three sets of data. The jets emanating from the two castellated nozzles exhibit reduced shock cell lengths when compared to the axisymmetric jet. Of the two castellated nozzles, the jet from the regular castellated nozzle has a marginally shorter shock cell length.

The three jets also differ in the magnitude of the peak velocity in each shock cell. The axisymmetric and divergent chamfered castellated nozzles produce jets with similar peak velocities in each shock cell. This is in contrast to the regular castellated nozzle, which has a much lower peak velocity in the jet. The lower peak velocity is likely to be due to increased shear layer thickness, which gives less efficient shock reflection. The jet produced by both of the castellated nozzles appears to decay more rapidly than the jet from the axisymmetric nozzle. There appears to be little evidence of a shock structure after $x/D = 9$, whereas the axisymmetric jet still has a shock structure at this downstream position.

CFD predictions of jets from the same three nozzles (Fig. 5) shows reasonable agreement with the experiments. The axisymmetric jet has the longest shock cell length, with the regular castellated nozzle producing the jet with the shortest shock cell length. The peak velocities in each shock cell are, however, much more similar for these three jets than they were in the experiments. The magnitude of the peak velocities is also predicted by the CFD to be significantly higher than was measured experimentally suggesting thinner shear layers. Additionally, the CFD model does not predict the early decay of the jets from the castellated nozzles. The CFD model predicted slightly longer individual shock cells than the LDV measurements. This is thought to be due partially to factors in the experiments, which were not represented in the CFD, notably jet oscillation and swirl [6].

4.2 Centreline Pitot Probe Measurements

Fig. 6 shows pitot probe measurements for the axisymmetric jet and jets from two of the castellated nozzles. The pitot probe data, p_{0p} were non-dimensionalised with ambient static pressure, p_a. Corresponding centreline static pressure measurements were not made, however, which meant that the usual Rayleigh correction for a stand-off normal shock in front of the probe could not be applied. In order to compare the pitot probe data with the CFD model, the CFD-predicted static pressure and Mach number were used in the normal shock equation to give the total pressure that a pitot probe would see if placed in the CFD-predicted flowfield assuming a stand-off normal shock [6]. Each set of pitot probe data is in two parts, labelled ‘nearfield’ and ‘farfield’, resulting from the enforced relocation of the traverse carriage.

The data show similar trends to the LDV measurements. The axisymmetric jet has the longest shock cell length with the jets from the two castellated nozzles exhibiting slightly shorter shock cell lengths. Of the two castellated nozzles tested, the convergent chamfered one appears to give the greatest reduction in shock cell length.

Comparison with the CFD predictions (Fig. 7) shows reasonable agreement. The CFD model predicts a higher pressure ratio in the first two shock cells than the experiments but the agreement is better in subsequent shock cells. Unfortunately the experimental measurements were not able to extend through the whole length of the shock core but the indications are that the CFD model is over-predicting the shock cell lengths, as was seen with the LDV data. The regular castellated nozzle is predicted to give a slightly shorter shock cell length than the convergent chamfered nozzle, however, the difference between the two designs is small.

4.3 Mixing Enhancement

Both the experimental measurements and the CFD model have indicated that the castellated nozzles produce jets with shorter shock cells than

the axisymmetric jet, however, it is still to be determined if this translates into enhanced jet mixing. For the purposes of this study, jet mixing is determined by a numerical integration of the mass flow rate passing through planes normal to the jet axis at various streamwise positions $(x/D = 2.5, 5, 7.5, 10, 15, 20)$. The edge of the integration plane has been chosen to be where $M = 0.06$. The results of this integration, as applied to the CFD data, are shown in Table 2.

At $x/D = 2.5$ all three castellated nozzles show an increased mass flow rate in the jet of between 6% and 9% when compared with the axisymmetric jet. At $x/D = 5$ this has increased to approximately 13% for the regular and divergent chamfered castellated nozzles. The convergent chamfered castellated nozzle shows a reduced mixing enhancement of only 2%. At $x/D = 7.5$ the level of mixing enhancement starts to deteriorate in the other nozzles as well, the divergent chamfered castellated nozzle offering the best enhancement with a 10% increase in mass flow rate. The mixing enhancement continues to reduce as downstream distance is increased until, beyond $x/D = 15$, the mass flow rate in the axisymmetric jet exceeds that in the jets from the castellated nozzles.

In order to gain some insight into the mechanism responsible for the mixing enhancement, contour plots of the Mach number at each streamwise plane were examined (Fig. 8). At $x/D = 2.5$, the cross-sectional shapes of the jets are very different. The divergent chamfered nozzle produces a jet with a lobe of high velocity fluid, which has been ejected radially through the gap in the castellations. Similar fluid ejections, but of slightly different shapes were observed for the other two castellated nozzle designs. It appears that a differential expansion of the jet fluid in the tooth and gap regions as it leaves the nozzle exit is responsible for the distorted jet shape. The positions of the nozzle lip and castellations are indicated on the figures.

Further downstream at $x/D = 5$ the lobed region of high velocity fluid has spread both radially and circumferentially for all three castellated nozzle designs. It is the divergent chamfered nozzle, however, which shows the greatest radial expansion, which correlates well with the higher level of mixing enhancement seem for this nozzle.

At a downstream distance of $x/D = 7.5$ viscous mixing is starting to force all three castellated nozzle jet cross-sections to a more circular shape. It appears that in doing so, the rate at which these jets can entrain ambient air is diminished (Table 2). By $x/D = 10$ only the divergent chamfered nozzle is showing any significant mixing enhancement over the axisymmetric one. As downstream distance is increased further, the mass flow rate in all four jets become, to within 2%, equal. At $x/D = 20$ all the jets have essentially a circular cross-section.

5 Conclusions

A study has been presented of the jet mixing from convergent nozzles with castellated lip geometries. A CFD calculation using the RNG k-ε turbulence model and solution-based mesh adaption has been shown to predict the main characteristics of the nearfield flow up to approximately 10 nozzle diameters downstream of the exit plane. Comparison with experimental LDV and pitot probe measurements shows broadly good agreement between all three techniques.

When compared with a plain axisymmetric jet, an increase, based on mass flow rate, of up to 13% in mixing was predicted for jets emanating from the castellated nozzles. The increased mixing rate of these jets appears to be due to differential expansion of the jet fluid in the gap and tooth regions as it leave the nozzle exit. This mixing enhancement was, however, confined to the nearfield flow $(x/D < 10)$. At greater streamwise distances viscous dissipation appeared to cause the entrainment mechanism to decay resulting in mixing rates lower than an axisymmetric jet with final mass flow rates similar in each case.

References

[1] Knowles K and Saddington A. J. Modelling and experiments on underexpanded turbulent jet

	Axisymmetric	Regular		Convergent		Divergent	
x/D	$\dot{m}\,(\mathrm{kgs}^{-1})$	$\dot{m}\,(\mathrm{kgs}^{-1})$	% change	$\dot{m}\,(\mathrm{kgs}^{-1})$	% change	$\dot{m}\,(\mathrm{kgs}^{-1})$	% change
0.0	0.638	0.642	0.6	0.643	0.8	0.640	0.3
2.5	0.745	0.811	8.9	0.796	6.8	0.790	6.0
5.0	0.867	0.975	12.5	0.884	2.0	0.982	13.3
7.5	1.012	1.080	6.7	1.011	−0.1	1.110	9.7
10.0	1.172	1.192	1.7	1.166	−0.5	1.220	4.1
12.5	1.377	1.361	−1.2	1.325	−3.8	1.417	2.9
15.0	1.582	1.547	−2.2	1.557	−1.6	1.541	−2.6
17.5	1.795	1.770	−1.4	1.749	−2.6	1.794	−0.1
20.0	2.025	1.982	−2.1	1.961	−3.2	2.016	−0.4
25.0	2.476	2.458	−0.7	2.440	−1.5	2.483	0.3
30.0	2.953	2.916	−1.3	2.897	−1.9	2.937	−0.5

Table 2 CFD prediction of the mass flow rate of the four nozzles at various streamwise planes.

mixing. *Proc 5th International Symposium on Engineering Turbulence Modelling and Measurement*, Mallorca, Spain, 16-18 September 2002.

[2] Knowles K and Wong R. Y. T. Passive control of entrainment in supersonic jets. *Proc RAeS Aerodynamics Research Conference*, pp 9.1–9.14, London, 17-18 April 2000.

[3] Miller P. Some experiments with high pressure free air jets. Technical Report BAe-KAD-N-GEN-3356, BAe plc., 1988.

[4] Pannu S. S and Johannesen N. H. The structure of jets from notched nozzles. *Journal of Fluid Mechanics*, Vol. 74, No 3, pp 515–528, 1976.

[5] Rodi W. *Turbulence Models and their Application in Hydraulics - A State of the Art Review*. 2nd edition, International Association for Hydraulic Research, Rotterdamseweg 185 - P.O. Box 177, 2600 MH Delft, The Netherlands, 1984.

[6] Saddington A. J and Knowles K. Simulation and experiments on under-expanded turbulent jets. *Proc CEAS Aerospace Aerodynamics Research Conference*, Cambridge, UK, 10-13 June 2002.

[7] Samimy M, Reeder M. F, and Zaman K. Supersonic jet mixing enhancement by vortex generators. *Proc AIAA/SAE/ASME/ASEE 27th Joint Propulsion Conference*, Sacramento, CA, USA, 24-26 June 1991. No. 91-2263.

[8] Samimy M, Zaman K. B. M. Q, and Reeder M. F. Effect of tabs on the flow and noise field of an axisymmetric jet. *AIAA Journal*, Vol. 31, No 4, pp 609–619, April 1993.

[9] Wong R. Y. T. *Enhancement of Supersonic Jet Mixing*. Ph.D. thesis, Department of Aerospace, Power and Sensors, Cranfield University, July 2000.

[10] Yakhot A and Orszag S. A. Renormalisation group analysis of turbulence: I. basic theory. *Journal of Scientific Computing*, Vol. 1, No 1, pp 1–51, 1986.

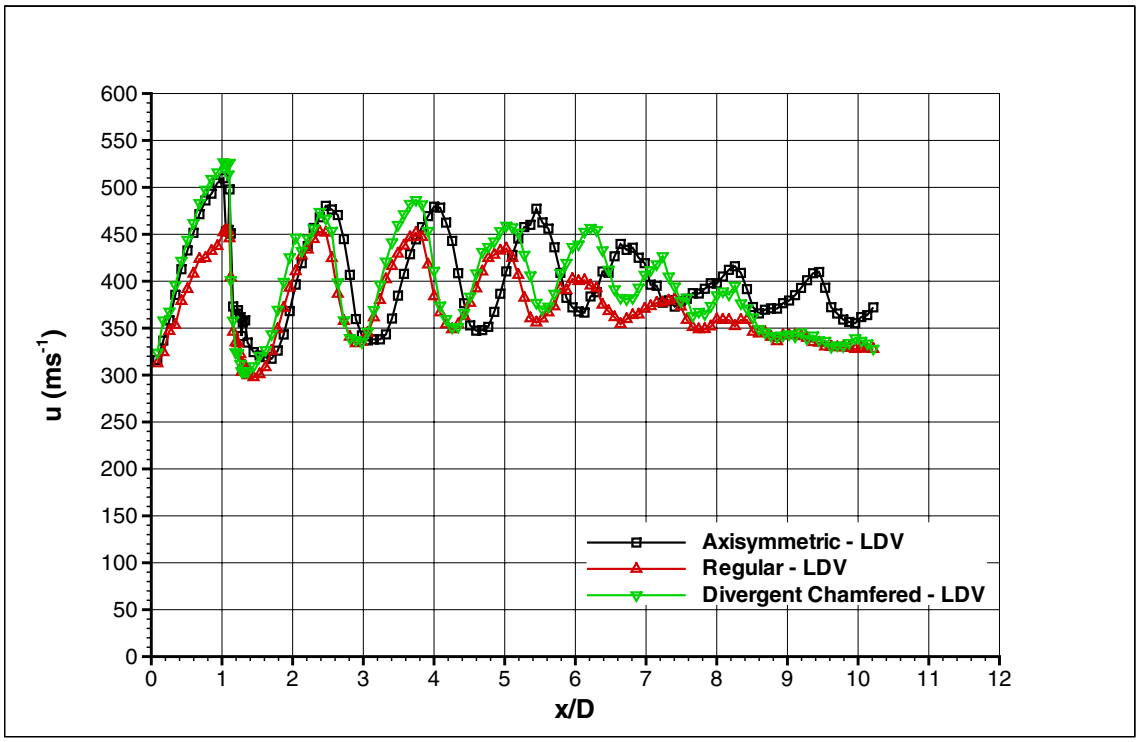

Fig. 4 Jet centreline axial velocity profiles, NPR = 4 (LDV).

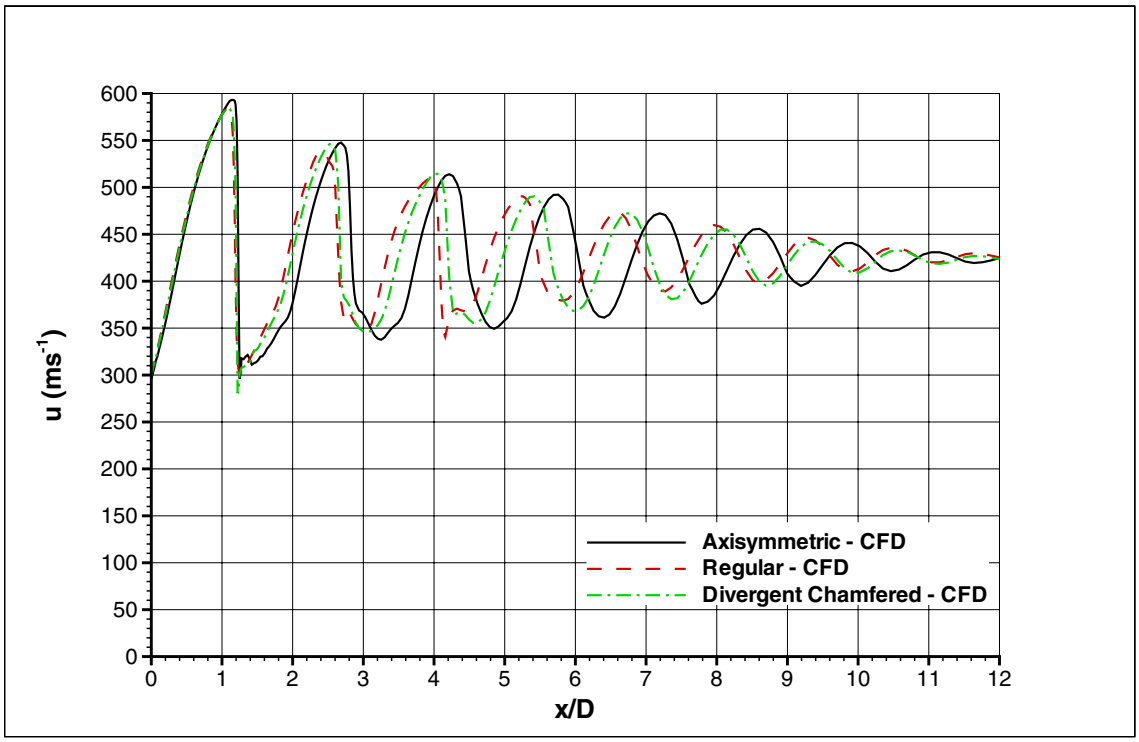

Fig. 5 Jet centreline axial velocity profiles, NPR = 4 (CFD).

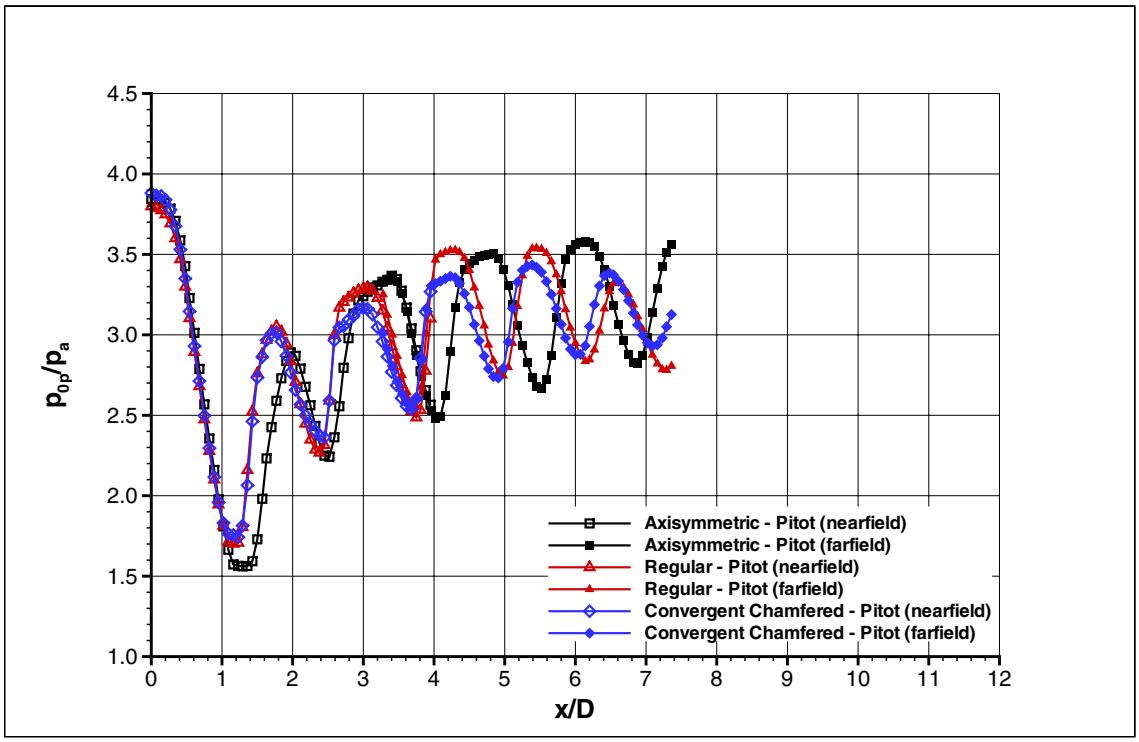

Fig. 6 Jet centreline pressure profiles, NPR = 4 (pitot probe).

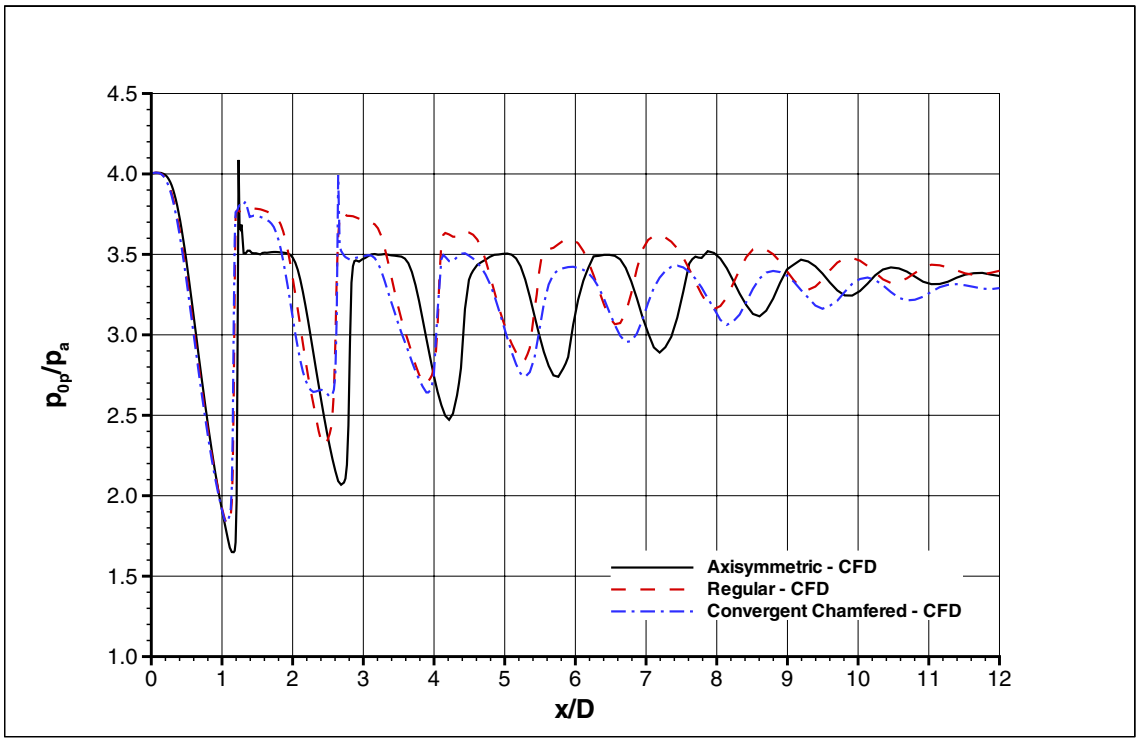

Fig. 7 Jet centreline pressure profiles, NPR = 4 (CFD).

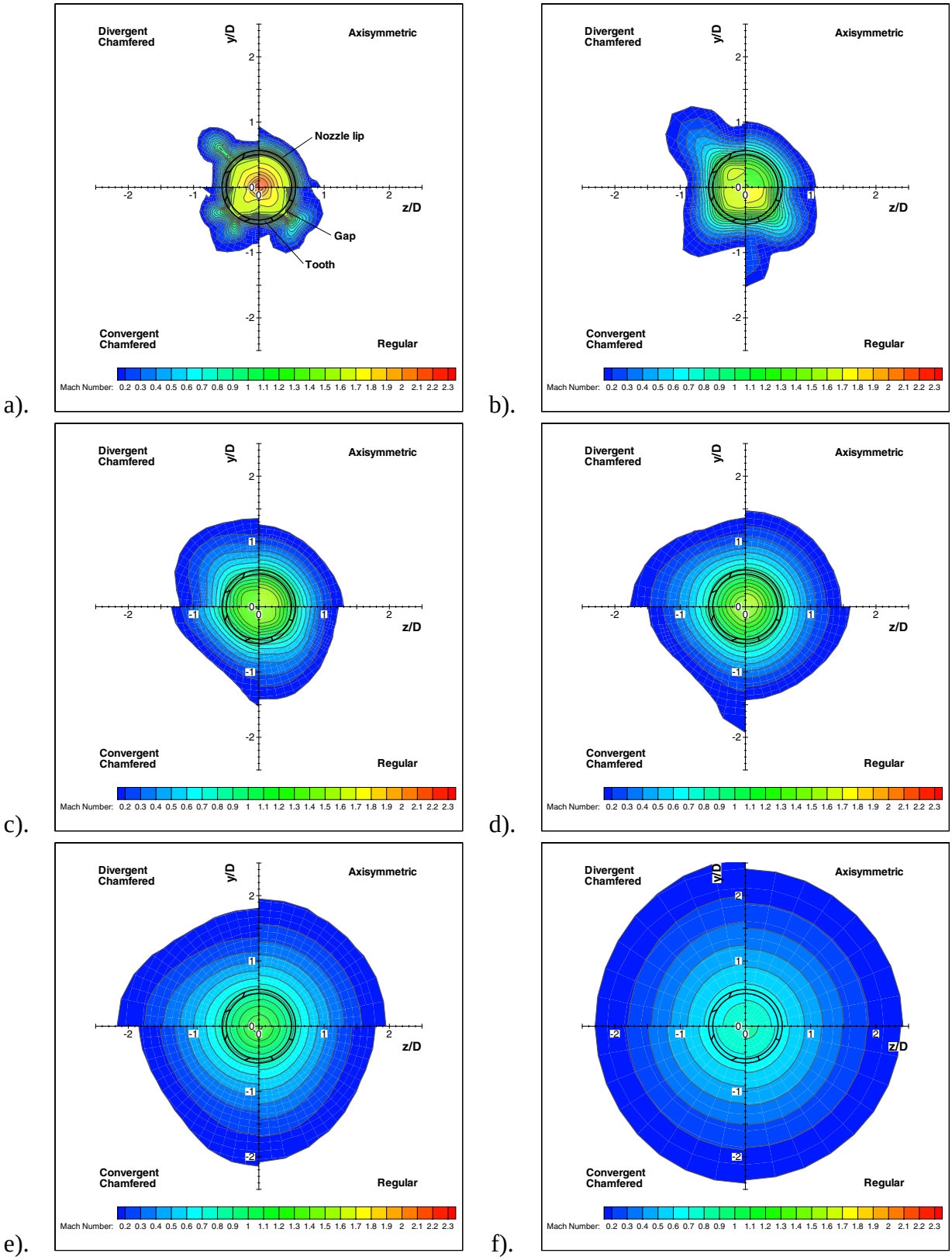

Fig. 8 CFD-predicted Mach number contours at various distances downstream of the nozzle exit: a). $x/D = 2.5$; b). $x/D = 5$; c). $x/D = 7.5$; d). $x/D = 10$; e). $x/D = 15$; f). $x/D = 20$.